TESTING CARBONATE FORMATION MECHANISMS AT NORTHEAST SYRTIS MAJOR USING MANUAL AND AUTOMATED HYPERSPECTRAL ANALYSES. M. S. Bramble[1], J. F. Mustard[1], and K. M. Cannon[1], [1]Department of Earth, Environmental, and Planetary Sciences, Brown University, Providence, RI, 02912 (Michael_Bramble@brown.edu).

Introduction: The Nili Fossae region of Mars hosts one of the largest geologic units on the planet showing enrichment in olivine at visible and infrared wavelengths [1–4]. This unit is part of a consistent stratigraphic package throughout the region where it overlays a phyllosilicate-bearing basement and is itself overlain by a capping unit lacking near-infrared absorptions [5]. The olivine-rich unit is particularly notable for its variable alteration to an olivine-carbonate-bearing assemblage [3,6,7]. Four formation mechanisms for this carbonate-bearing assemblage have been proposed: (1) Alteration of olivine in ultramafic rocks by the subsurface percolation of groundwater at slightly elevated temperatures from the geothermal gradient [6]. (2) Weathering of olivine-rich rocks exposed at the surface by a water-limited system, or at ambient conditions in a manner akin to the alteration of meteorites in Antarctica [6]. (3) Precipitation of the carbonate from ephemeral lakes [6]. (4) Formation of carbonate, serpentine, and talc during a single metamorphic event in a zone of alteration at the contact between underlying phyllosilicate-rich rocks and overlying heated olivine-rich rocks [6,8,9]. These four hypotheses each have unique predictions for the mineral species present, their stratigraphic position, and the geomorphology of mineral host units (**Figure 1**), with the type and stratigraphic position of the phyllosilicate being a main distinguishing factor. Knowing what mechanism formed the carbonate in Nili Fossae will have major implications for constraining the possible amount of atmospheric CO_2 sequestered in geological formations and therefore provide inferences for the early climate of Mars.

Methods: Our manual analysis of hyperspectral Compact Reconnaissance Imaging Spectrometer for Mars (CRISM) data followed methods described previously (e.g., [3,7]). We focus on three CRISM observations in the Northeast Syrtis Major region, FRT0001821C, FRT00019538, and FRT00023728, which cover well-exposed erosional windows through the olivine-rich unit. We targeted pixels in close proximity to the contact between the upsection olivine-rich unit, and the downsection phyllosilicate-bearing basement. Building on the methods of [10] and [11], we also applied hybrid Hapke radiative transfer modeling methods [12] to unmix the images. Endmembers and CRISM pixels were converted to single-scattering albedo and then linearly unmixed using a least-squares approach and non-negative and sum-to-one constraints. Four non-physical endmembers were used consisting of a bright endmember with unity at all wavelengths, a dark endmember with a near-zero value at all wavelengths, and positive and negative slope endmembers. A single in-scene endmember consisting of the mean of the detector column was also applied. Laboratory endmembers of fayalite, saponite, nontronite, talc, and magnesite were iteratively added to the endmember library. F-test values were calculated between the RMSE of the fit with and without the laboratory endmembers, and only if the fit was improved above a critical threshold was the added laboratory endmember result recorded. Maps were generated where each pixel corresponds to the endmember mineralogy with the highest F-test value (filtered to only include mineral spectral fractions >5%). Ongoing work involves applying a second approach for comparison, where, in place of the mean column endmember, user-defined in-scene endmembers will be used from the dark-toned capping unit and a spectrally 'pure' olivine-rich unit without alteration mineral absorptions.

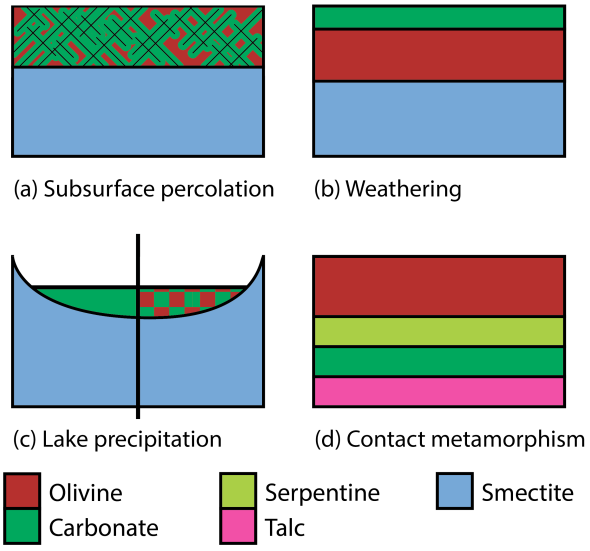

Figure 1: Simplified near-infrared mineral stratigraphy resulting from the four proposed carbonate formation hypotheses suggested for Nili Fossae. Schematic shows the relative stratigraphic positions. The individual strata are not necessarily to scale.

Results: From our manual analyses (**Figure 2a**), we arrive at several observations do not support the widespread presence of talc in the downsection unit, including: (1) the mineral talc does not have H_2O in its

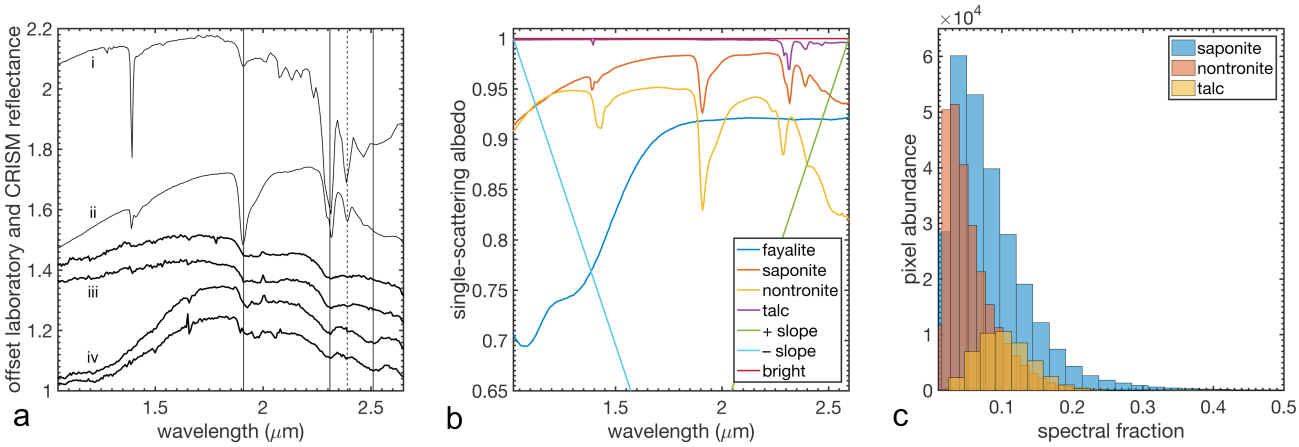

Figure 2: (a) Manual analysis results. Laboratory spectra for talc (i) and saponite (ii) are shown in comparison to two spectra collected from the downsection basement (iii) and two from the olivine-rich unit (iv). Vertical lines are at 1.91, 2.31, 2.39, and 2.51 μm. (b) Selection of laboratory and non-physical endmembers used in unmixing procedures. (c) Histogram of unmixing results showing the abundance of CRISM pixels with a given phyllosilicate spectral fraction in the three scenes analyzed. Values of zero are omitted.

structure and therefore cannot explain the ubiquitous absorption at ~1.9 μm; (2) talc has a sharp and deep 1.39 μm absorption from OH vibration and a broader 1.44 μm absorption absent here; (3) narrow absorptions at 2.315 and 2.386 μm of talc are of comparable width and the latter is ~50% the depth of the former and are absent here [13]; (4) talc has a 2.466 μm absorption ~50% the band depth of the 2.386 absorption [13] that has not been observed in our analyses; and (5) talc has a deep gap between the local 2.2 and 2.42 μm continuum and the septum at 2.35 μm [9], and this septum is largely absent or much weaker than in laboratory talc or saponite. If a 2.39 μm absorption alone was diagnostic of talc, our observations would suggest that talc is present in detectable quantities in both the olivine-rich unit and the downsection basement. As an ~1.9 μm absorption is always observed when the 2.39 μm absorption is observed, the simplest interpretation is that a smectite is present. The morphology of the olivine-carbonate-bearing unit rules out the lake precipitation hypothesis as this unit drapes both topographic highs and lows.

The CRISM scenes were successfully unmixed using the combination of non-physical, in-scene, and laboratory endmembers (**Figure 2b**). All non-physical endmembers were modeled at spectral fractions ≤3%. The mean column endmembers had the highest spectral fractions (~85%) as expected, because this endmember accounts for most of the spectral variability in the scene. Lastly, the phyllosilicates saponite, nontronite, and talc were modeled in decreasing spectral fractions (**Figure 2c**). Smectites are modeled in both the olivine-rich unit and the downsection basement. Talc is only modeled in isolated patches in the downsection basement, with smectites at higher spectral percentages in the downsection basement than talc in all unmixing runs, and in many talc was modeled at near-zero values. The automated results collectively suggest that smectites can be regularly unmixed from the spectra of the scene studied, and in all metrics analyzed smectites are the preferred phyllosilicate and they are present in both units investigated.

Discussion and Implications: We argue that the results from our near-infrared spectroscopic analyses provide several lines of evidence in favor of the presence smectites over talc in the local basement. If we were to use these observations to suggest that smectites are the dominant phyllosilicate in the downsection basement, this would add support that carbonate formed in situ within the olivine-rich unit at low temperatures, such as by surface weathering or subsurface percolation of waters, and not by a high temperature, talc-carbonate, contact metamorphism system. Furthermore, this would corroborate recent results north-northeast of our analysis area where a similar in situ alteration reaction was favored and modest carbonate abundances calculated [14].

References: [1] Hoefen T.M. et al. (2003) *Science, 302,* 627–630. [2] Mustard J.F. et al. (2007) *JGR, 112,* E08S03. [3] Mustard J.F. et al. (2009) *JGR, 114,* E00D12. [4] Ody A. et al. (2013) *JGR, 118*, 234–262. [5] Mangold N. et al. (2007) *JGR, 112,* E08S04. [6] Ehlmann B.L. et al. (2008) *Science, 322,* 1828–1832. [7] Ehlmann B.L. et al. (2009) *JGR, 114,* E00D08. [8] Brown A.J. et al. (2010) *EPSL, 297,* 174–182. [9] Viviano C.E. et al. (2013) *JGR, 118,* 1858–1872. [10] Cannon K.M. and Mustard J.F. (2015) *Geology, 43,* 635–638. [11] Goudge T.A. et al. (2015) *Icarus, 250,* 165–187. [12] Hapke B. (1981) *JGR, 86,* 3039–3054. [13] Clark R.N. et al. (2007) USGS digital spectral library splib06a. [14] Edwards C.S. and Ehlmann B.L. (2015) *Geology*, *43*, 863–866.